

MEASURING DIRECTED INTERACTIONS USING CELLULAR NEURAL NETWORKS WITH COMPLEX CONNECTION TOPOLOGIES

H. DICKTEN^{1,2,3,*}, C. E. ELGER¹, K. LEHNERTZ^{1,2,3}

¹*Department of Epileptology, University of Bonn,
Sigmund-Freud-Straße 25, 53105 Bonn, Germany*

²*Helmholtz-Institute for Radiation and Nuclear Physics, University of Bonn,
Nussallee 14–16, 53115 Bonn, Germany*

³*Interdisciplinary Center for Complex Systems, University of Bonn,
Brühler Straße 7, 53175 Bonn, Germany*

**E-mail: hdickten@uni-bonn.de*

We advance our approach of analyzing the dynamics of interacting complex systems with the nonlinear dynamics of interacting nonlinear elements. We replace the widely used lattice-like connection topology of cellular neural networks (CNN) by complex topologies that include both short- and long-ranged connections. With an exemplary time-resolved analysis of asymmetric nonlinear interdependences between the seizure generating area and its immediate surrounding we provide first evidence for complex CNN connection topologies to allow for a faster network optimization together with an improved approximation accuracy of directed interactions.

Keywords: CNN; Directed Interactions; Nonlinear Interdependence; iEEG; Complex Networks; Time Series Analysis; Seizure Prediction Device

1. Introduction

Synchronization phenomena play an important role in nearly all fields of science, including physics, chemistry, economy, and the neurosciences.^{1,2} The human epileptic brain can be regarded as a prominent example in which different forms of synchronization can be observed. Estimators for synchronization^{3,4} are highly attractive to characterize interactions between brain areas involved in ictogenesis.

Promising computational platforms for approximating these estimators are, among other approaches,⁵ Cellular Neural (or Nonlinear) Networks (CNN) as they are capable of universal computation and offer massive computing power while minimizing space and energy consumption and are

already available as analogue integrated circuits.^{6–9} Recent studies have shown that the approach of analyzing the dynamics of interacting complex systems with the nonlinear dynamics of interacting nonlinear elements can also be extended to the concepts of phase synchronization¹⁰ and generalized synchronization.¹¹ With the latter concept symmetric and asymmetric nonlinear interdependence measures can be defined that allow one to characterize strength and direction of interactions.^{11–15}

We investigated whether a CNN-based characterization of directed interactions can further be improved by modifying the canonical Chua–Yang CNN.¹⁶ This CNN consists of a regular (lattice-like) arrangement of cells which we replace by complex topologies.^{17,18} We evaluate approximation accuracies through the analysis of directed interactions in long-term, multi-channel, intracranial electroencephalographic (iEEG) recordings from an epilepsy patient.

2. Methods

2.1. *Nonlinear Interdependencies*

Let A and B denote two dynamical systems and let $a_n, n = 1, \dots, N$ and $b_n, n = 1, \dots, N$ denote time series of some observable of the respective system. With

$$\vec{a}_n = (a_n, \dots, a_{n-(d_e-1)\tau}) \quad \text{and} \quad \vec{b}_n = (b_n, \dots, b_{n-(d_e-1)\tau}) \quad (1)$$

we denote the reconstructed delay vectors in state space^{19,20} with an appropriate chosen time delay τ and embedding dimension d_e . Given some reference point in state space, the mean-squared Euclidean distance to its k nearest neighbors reads:

$$R_n^{(k)}(A) = \frac{1}{k} \sum_{j=1}^k (\vec{a}_n - \vec{a}_{r_{n,j}})^2, \quad (2)$$

where $r_{n,j}, j = 1, \dots, k$ denote the time indices of the k nearest neighbors of \vec{a}_n . With $s_{n,j}, j = 1, \dots, k$ as time indices of the k nearest neighbors of \vec{b}_n , $R_n^{(k)}(B)$ is defined analogously. In addition, the *B-conditioned* mean-squared Euclidean distance in the state space of system A is derived by replacing the nearest neighbors of \vec{a}_n by the equal-time partners of the nearest neighbors of \vec{b}_n :

$$R_n^{(k)}(A|B) = \frac{1}{k} \sum_{j=1}^k (\vec{a}_n - \vec{a}_{s_{n,j}})^2. \quad (3)$$

$R_n^{(k)}(B|A)$ is defined in complete analogy, and the nonlinear interdependence $S^{(k)}$ then reads¹²

$$S^{(k)}(A|B) = \frac{1}{M} \sum_{n=1}^M \frac{R_n^{(k)}(A)}{R_n^{(k)}(A|B)}, \quad (4)$$

where M denotes the total number of state space vectors. Strength and direction of interactions can be characterized via a symmetric and asymmetric measure:

$$\begin{aligned} S_{\text{symm}}^{(k)} &= \frac{S^{(k)}(A|B) + S^{(k)}(B|A)}{2} \\ S_{\text{asymm}}^{(k)} &= \frac{S^{(k)}(A|B) - S^{(k)}(B|A)}{2}. \end{aligned} \quad (5)$$

2.2. Cellular Neural Networks (CNN)

Artificial Neural Networks (ANNs) are computational tools inspired by the brain that have found extensive utilization in complex real-world problems.²¹ An ANN consists of simple artificial *cells* or *processing units* which are connected via *edges*, but there exists no single formal definition of what an ANN exactly is. ANNs feature characteristics such as high parallelism, intrinsic nonlinearity, as well as fault and noise tolerance. More importantly, ANNs can be trained using a set of given examples and offer the ability to generalize.^{22,23}

A Cellular Neural Network (CNN) is a subset of ANN where—in contrast to a Hopfield network²⁴—only local connections between cells are allowed.¹⁶ Hence the number of edges increases only linearly with the number of cells of the network.

2.2.1. Dynamics of a CNN

Following Ref. 25, a CNN is a spatial arrangement of locally connected cells, where each cell is a dynamical system which has an input u , bias z , output $y(t)$ and state $x(t)$ evolving according to some state equation (cf. Fig. 1).

Let us first consider a CNN which consists of a two-dimensional $\mathcal{M} \times \mathcal{N}$ translation-invariant lattice of cells with nonlinear interactions. The corresponding state equation for cell (i, j) ($i \in [1, \mathcal{M}]$ and $j \in [1, \mathcal{N}]$) reads

$$\dot{x}_{ij}(t) = -x_{ij}(t) + \sum_{lm \in \mathcal{I}_{ij}} \mathcal{A}_{lm}(y_{lm}(t)) + \sum_{lm \in \mathcal{I}_{ij}} \mathcal{B}_{lm}(u_{lm}) + z, \quad (6)$$

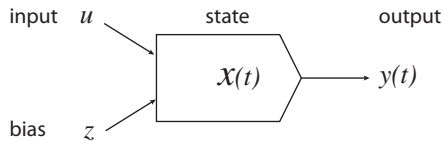


Fig. 1. Representation of a single cell of a CNN. Each cell is a dynamical system with state $x(t)$ evolving according to some state equation.

where \mathcal{I}_{ij} denotes the *sphere of influence* of cell (i, j) , and $l, m \in \mathcal{I}_{ij}$. \mathcal{A}_{lm} and \mathcal{B}_{lm} denote the feedback and feed-forward template functions, respectively. In order to present the time series $a_n, b_n, N = 4096$ to the network, we used a line wise alignment, i.e., the rightmost cell in a row is connected to the leftmost cell in the following row. Time series a_n was assigned to the input u and time series b_n to the initial state $x(0)$ of the CNN. Together with the chosen boundary condition this alignment preserves the temporal order of the time series. Nevertheless it may introduce correlations between uncorrelated data points within the time series.

Following Ref. 11, we here define the canonical Chua–Yang CNNcan as a quadratic network arrangement ($\mathcal{M} \times \mathcal{N} = 64$) with a minimum possible 3×3 sphere of influence as well as polynomial-type template functions of order three (cf. Fig. 2 left). In order to investigate whether complex connection topologies allow for an improved CNN-based characterization of directed interactions, we additionally consider two modified versions of CNNcan:

With CNNlr we define a topology, in which some short- and long-ranged connections between cell (i, j) and cells of its sphere of influence are introduced. The distance of the long-ranged connections corresponds to the time of the first maximum of the autocorrelation function of time series a_n and b_n , respectively (normalized by the sampling interval), thus minimizing the aforementioned effect of connecting possibly uncorrelated data. Short-ranged connections exist between cells (i, j) and $(i, j - 1)$ and between cells (i, j) and $(i, j + 1)$ (cf. Fig. 2 middle). Eventually we fully relax the canonical topology by choosing connections between cell (i, j) and eight other cells (that comprise the sphere of influence) at random (CNNran; cf. Fig. 2 right). Each sphere of influence remained translation-invariant and consisted of nine (eight to other cells and one to itself) connections to ensure comparability between different topologies.

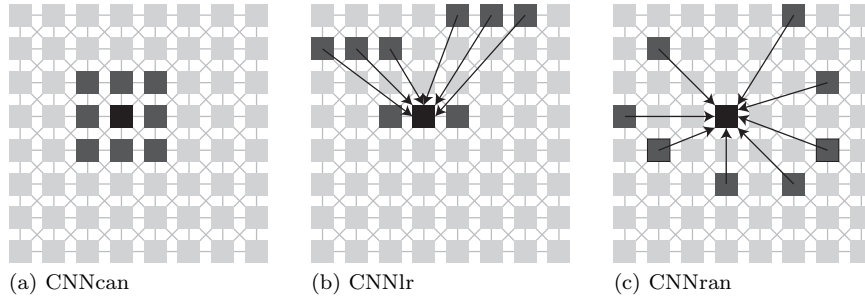


Fig. 2. CNN with the canonical (a) and with complex connection topologies (b and c). In (b) long-ranged connections are chosen according to the time of the first maximum of the autocorrelation function for each time series separately. In (c) short- and long-ranged connections are chosen at random.

2.2.2. Optimization and Validation

In the following, we denote with U , $X(t)$, and $Y(t)$ the inputs, states and outputs of all CNN cells. In order to optimize the networks we used an evolutionary algorithm^{26,27} with the following parameters: population size: 50, number of survivors: 10, number of immigrants: 10, maximum number of iteration steps: 300.

We performed an in-sample optimization of our CNN using $V = 20$ representative pairs of time series of 20.48s duration (in total ≈ 7 min EEG) each along with the corresponding value of the nonlinear interdependence measure calculated according to Eq. (5) (denoted as S^{ref} in the following) with $\tau = 5$, $d_e = 10$, and $k = 6$. Half of the values represented weakly dependent time series ($S_{\text{asymm.}}^{\text{ref. low}} \in [-0.04, -0.02]$), and the other half stronger dependent time series ($S_{\text{asymm.}}^{\text{ref. high}} \in [0.04, 0.06]$), respectively.²⁸ To check for possible over-optimization of our CNN, we performed an additional out-of-sample validation using a similar setup as before but with another set of 20 pairs of time series along with the corresponding values of the nonlinear interdependence.

The approximated asymmetric nonlinear interdependence measure $S_{\text{asymm.}}^{(k)}$ was obtained by the rescaled mean output of all cells:

$$S_{\text{asymm.}}^{\text{CNN}} = \left(\frac{S_{\text{asymm.}}^{\text{ref. high}} - S_{\text{asymm.}}^{\text{ref. low}}}{\mathcal{MN}} \sum_{i,j=0}^{\mathcal{M},\mathcal{N}} \frac{y_{i,j}(\tau_{\text{trans}}) + 1}{2} \right) + S_{\text{asymm.}}^{\text{ref. low}} \quad (7)$$

After choosing random initial values for the components of templates \mathcal{A} and \mathcal{B} and for the global cell bias z the global error was minimized:

$$E_g = \frac{1}{V} \sum_{v=0}^{V-1} \left(\frac{1}{4\mathcal{M}\mathcal{N}} \sum_{i,j=0}^{\mathcal{M},\mathcal{N}} (y_{i,j,v}(\tau_{\text{trans}}) - Y_v^{\text{ref}})^2 \right) \quad (8)$$

where τ_{trans} denotes some fixed transition time.^{29,30} All calculations were performed using our distributed computing system,³¹ and network simulations were performed with Conedy.³²

3. CNN-based iEEG Analysis

We analyzed directed interactions in multi-channel iEEG recordings from an epilepsy patient who underwent presurgical evaluation of a left-sided mesial temporal lobe epilepsy. After selective amygdalo-hippocampectomy the patient is completely seizure-free. The patient had signed informed consent that the clinical data might be used and published for research purposes. The study protocol had previously been approved by the ethics committee of the University of Bonn. iEEG was measured from bilaterally implanted intrahippocampal depth electrodes. iEEG data were sampled at 200 Hz using a 16 bit analog-to-digital converter and filtered within a frequency band of 0.5–85 Hz.

In the following we report our findings of estimating directed interactions between the seizure generating area and its immediate surrounding in a time-resolved manner (moving window analysis; non-overlapping windows of 20.48 s duration). We here restrict ourselves to an interictal recording lasting for about 25 hours.

First of all we note that short- and long-term fluctuations of nonlinear interdependencies between brain regions could well be approximated even with CNN with complex connection topologies. This observation does not only extend previous findings¹¹ but it also indicates that the use of complex topologies leads to a faster optimization and validation of the CNN (cf. upper parts of Fig. 3–5). More importantly, when comparing performance data of the three investigated CNN, approximation accuracy increased from 87.5 % (CNNcan) to 90.1 % (CNNran) to 92.7 % (CNNlr) (cf. lower parts of Fig. 3–5).

4. Conclusion

We have investigated whether a CNN-based approximation of directed interactions between the dynamics of different areas of the human epileptic brain can be improved by replacing the lattice-like arrangement of CNN

cells by complex connection topologies. Findings obtained from an exemplary analysis of directed interactions in intracranial electroencephalographic recordings from an epilepsy patient indicate that complex connection topologies allow for a faster optimization of CNN together with an improved approximation accuracy of nonlinear interdependence. Our preliminary though promising findings need to be validated on the data from a larger group of patients.

Although our findings are, at present, restricted to simulated or digital realizations of CNN, their powerful computational capacity and generalization capability combined with small size and low power consumption of hardware realizations render these networks highly attractive for the development of miniaturized seizure prediction devices.

Acknowledgments

This work was supported by the Deutsche Forschungsgemeinschaft (Grand No. LE660/2-4).

References

1. A. S. Pikovsky, M. G. Rosenblum and J. Kurths, *Synchronization: A universal concept in nonlinear sciences* (Cambridge University Press, Cambridge, UK, 2001).
2. S. Boccaletti, J. Kurths, G. Osipov, D. L. Valladares and C. S. Zhou, *Phys. Rep.* **366**, 1 (2002).
3. K. Lehnertz, S. Bialonski, M.-T. Horstmann, D. Krug, A. Rothkegel, M. Staniek and T. Wagner, *J. Neurosci. Methods* **183**, 42 (2009).
4. K. Lehnertz, *Physiol. Meas.* **32**, 1715 (2011).
5. K. Abdelhalim, V. Smolyakov and R. Genov, *IEEE Trans. Biomed. Circuits Syst.* **5**, 430 (2011).
6. L. O. Chua and T. Roska, *Cellular neural networks and visual computing* (Cambridge University Press, Cambridge UK, 2002).
7. A. Chernihovskyi, F. Mormann, M. Müller, C. E. Elger, G. Baier and K. Lehnertz, *J. Clin. Neurophysiol.* **22**, 314 (2005).
8. R. Tetzlaff, T. Niederhofer and P. Fischer, *Int. J. Circ. Theor. Appl.* **34**, 89 (2006).
9. T. Roska, *Int. J. Circ. Theor. Appl.* **36(5-6)**, 523 (2008).
10. R. Sowa, A. Chernihovskyi, F. Mormann and K. Lehnertz, *Phys. Rev. E* **71**, 061926 (2005).
11. D. Krug, H. Osterhage, C. E. Elger and K. Lehnertz, *Phys. Rev. E* **76**, 041916 (2007).
12. J. Arnhold, P. Grassberger, K. Lehnertz and C. E. Elger, *Physica D* **134**, 419 (1999).
13. D. Chicharro and R. G. Andrzejak, *Phys. Rev. E* **80**, 026217 (2009).

14. R. G. Andrzejak, D. Chicharro, K. Lehnertz and F. Mormann, *Phys. Rev. E* **83**, 046203 (2011).
15. K. Lehnertz, D. Krug, M. Staniek, D. Glüsenkamp and C. E. Elger, Preictal directed interactions in epileptic brain networks, in *Epilepsy: The Intersection of Neurosciences, Biology, Mathematics, Engineering and Physics*, eds. I. Osorio, H. Zaveri, M. Frei and S. Arthurs (CRC Press, Boca Raton, FL, 2011) pp. 265–272.
16. L. O. Chua and L. Yang, *IEEE Trans. Circuits Syst.* **35**, 1257 (1988).
17. D. J. Watts and S. H. Strogatz, *Nature* **393**, 440 (1998).
18. K. Tsuruta, Z. Yang, Y. Nishio and A. Ushida, *IEIC Technical Report* **103**, 67 (2003).
19. H. Whitney, *Ann. Math.* **37**, 645 (1936).
20. F. Takens, Detecting strange attractors in turbulence, in *Dynamical Systems and Turbulence (Warwick 1980)*, eds. D. A. Rand and L.-S. Young, Lecture Notes in Mathematics, Vol. 898 (Springer-Verlag, Berlin, 1981) pp. 366–381.
21. K. Priddy and P. Keller, *Artificial neural networks: an introduction* (SPIE Press, Bellingham, WA, 2005).
22. T. L. H. Watkin, A. Rau and M. Biehl, *Rev. Mod. Phys.* **65**, 499 (1993).
23. S. Haykin, *Neural Networks - A Comprehensive Foundation*, 10 edn. (Tom Robbins, London, UK, 1999).
24. J. Hopfield, *Proc. Natl. Acad. Sci. U.S.A.* **79**, 2554 (1982).
25. L. O. Chua, *CNN: A paradigm for complexity* (Singapore: World Scientific, 1998).
26. J. H. Holland, *Adaptation in natural and artificial systems* (The University of Michigan Press, Ann Arbor, USA, 1975).
27. R. Kunz, A. Loncar and R. Tetzlaff, SCNN 2000, Part I and II, in *Proceedings of the 6th IEEE International Workshop on Cellular Neural Networks and Their Applications*, ed. L. Fortuna (IEEE Press, Piscataway, NJ, 2000).
28. D. Krug, C. E. Elger and K. Lehnertz, A CNN-based synchronization analysis for epileptic seizure prediction: Inter- and intraindividual generalization properties, in *11th International Workshop on Cellular Neural Networks and Their Applications, 2008.*, eds. D. Vilarino, D. Ferrer and V. Brea Sanchez (IEEE Press, Piscataway, NJ, 2008).
29. R. Kunz, R. Tetzlaff and D. Wolf, Brain electrical activity in epilepsy: Characterization of the spatio-temporal dynamics with cellular neural networks based on a correlation dimension analysis, in *Proceedings of the IEEE International Symposium on Circuits and Systems*, eds. J. Vandevale and M. Hasler (IEEE Press, Piscataway, NJ, 2000).
30. D. Krug, A. Chernihovsky, H. Osterhage, C. E. Elger and K. Lehnertz, Estimating generalized synchronization in brain electrical activity from epilepsy patients with cellular nonlinear networks, in *Proc. 10th IEEE International Workshop on Cellular Neural Networks and their Applications*, eds. V. Tavsanoglu and S. Arik (IEEE Press, Piscataway, NJ, 2006).
31. A. Müller, H. Osterhage, R. Sowa, R. G. Andrzejak, F. Mormann and K. Lehnertz, *J. Neurosci. Methods* **152**, 190 (2006).
32. A. Rothkegel and K. Lehnertz, *Chaos* **22**, 013125 (2012).

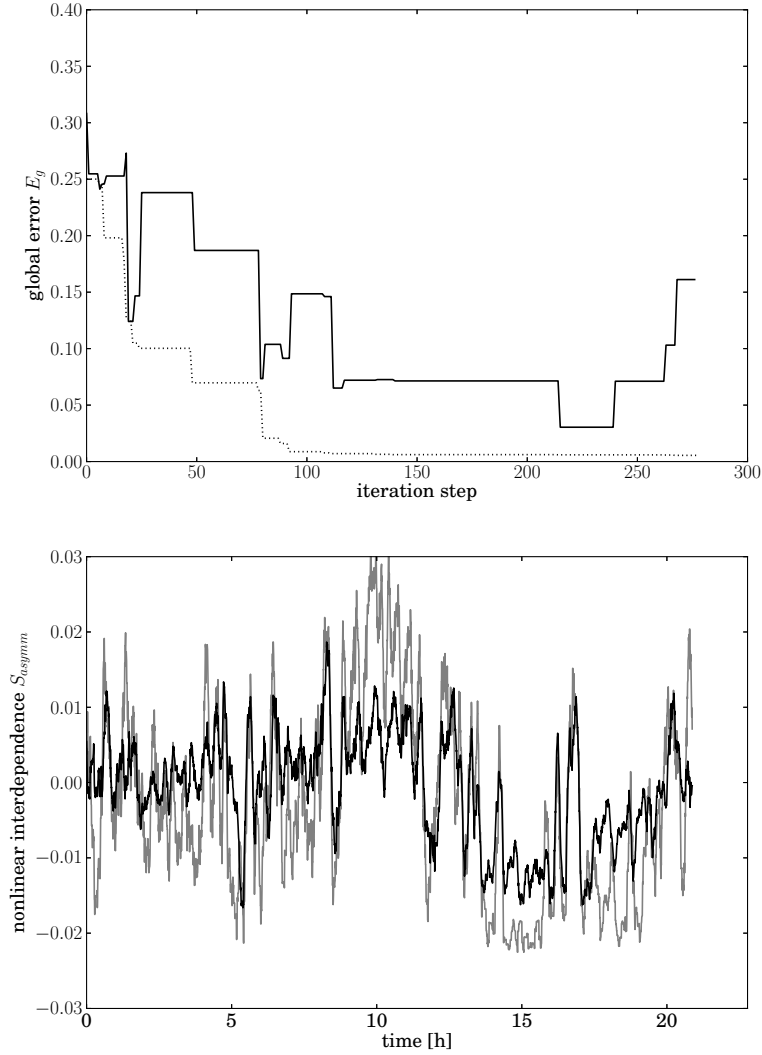


Fig. 3. Exemplary findings obtained with CNNcan. Top: Global error E_g (cf. Eq. (8)) depending on the number of iteration steps during in-sample optimization (dotted line) and during out-of-sample validation (solid line). Bottom: Temporal evolution of analytically calculated (black line) and approximated nonlinear interdependence S_{asyymm} (gray line) between the seizure generating area and its immediate surrounding. Profiles are smoothed using a 15-point (≈ 5 min) moving-average filter for better visualization. The CNN-approximation was performed with the templates \mathcal{A} and \mathcal{B} and the global cell bias z obtained in iteration step 80.

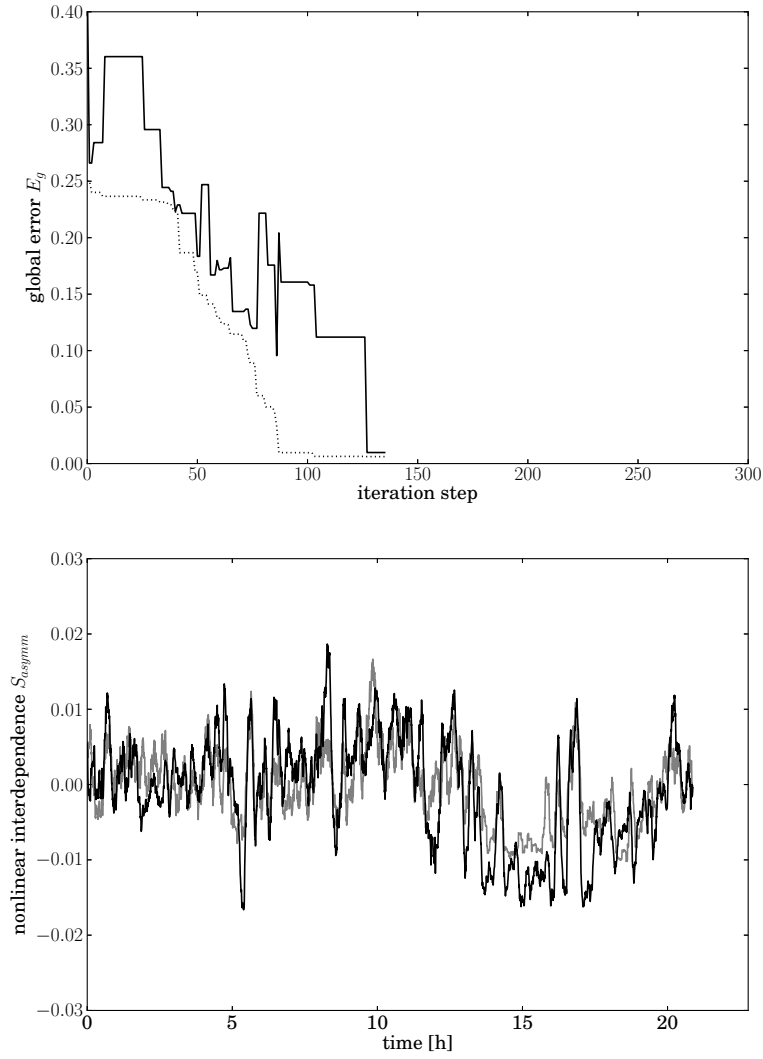


Fig. 4. Same as Fig. 3 but for CNNr. The CNN-approximation of the nonlinear interdependence S_{asymm} was performed with the templates \mathcal{A} and \mathcal{B} and the global cell bias z obtained in iteration step 58.

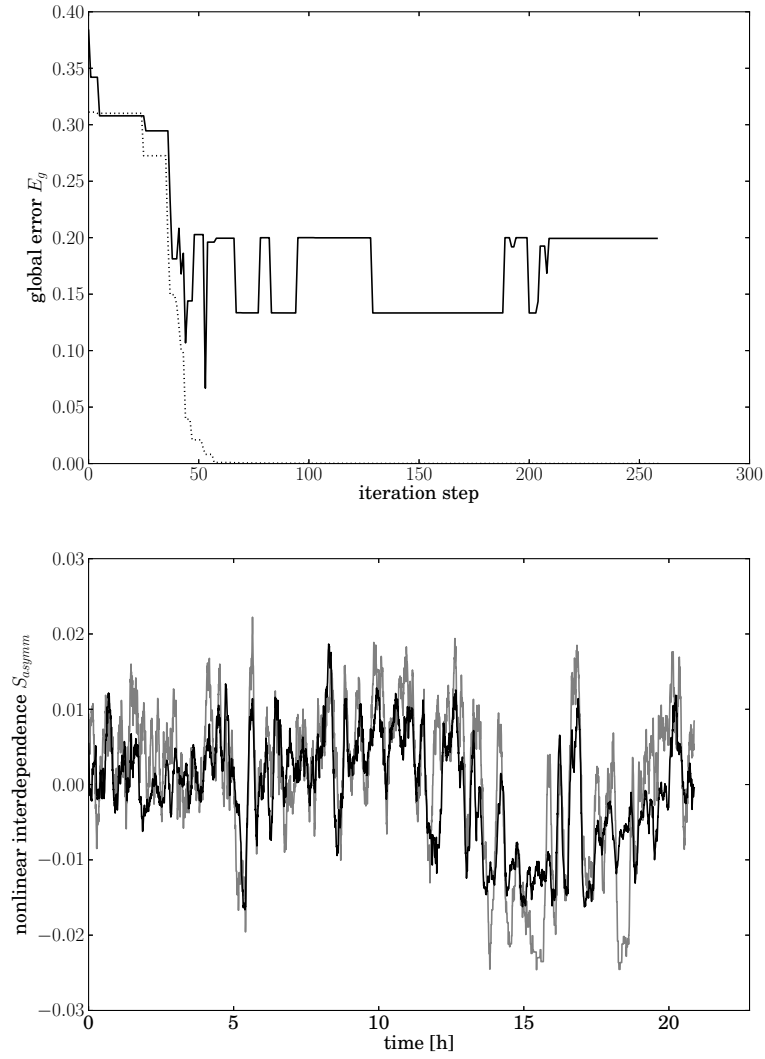


Fig. 5. Same as Fig. 3 but for CNNran. The CNN-approximation of the nonlinear interdependence S_{asymm} was performed with the templates \mathcal{A} and \mathcal{B} and the global cell bias z obtained in iteration step 40.